# FGAN CONTRIBUTION TO THE MIR DEORBITING CAMPAIGN 2001

**L. Leushacke**

*FGAN - Research Institute for High Frequency Physics and Radar Techniques (FHR), Neuenahrer Str. 20, 53343 Wachtberg–Werthhoven, Germany*

## ABSTRACT

Radar is well suited for the observation of Earth orbiting objects. Especially in the case of reentering spacecraft frequent observations from many systems at different locations are necessary for accurate prediction of reentry windows and risk assessment.
For the case of the MIR station, which was the first controlled deorbiting of a large scale space vehicle, measurement data are important for the verification of orbital and attitude maneuvres and in the emergency case of a loss of control.
In January 2001 the German Ministry of Defense (BMVg) agreed upon requests from the Ministry of the Interior (BMI) and national/international space agencies to give support to the operation centres and analysis teams by measurements of MIR with FGAN's Tracking and Imaging Radar (TIRA) system.
Tracking data should be provided in the form of orbital element sets as well as observation vector sequences and should timely be transfered to a data dissemination centre to be implemented at ESA/ESOC.
Furthermore high resolution radar images and image sequences should be gained for the analysis of the station's status and stabilization and for the verification of attitude maneuvres.
After a brief introduction of the TIRA system and a discussion on the kind and quality of information gained from TIRA measurement data and on the routines developed for timely data processing and transfer, an overview about the TIRA observations of the MIR station from January to March will be given. Presented results will mainly focus on attitude analysis from radar images. Some of the drawbacks and unsolved problems will also be shortly discussed.

## 1. THE TIRA SYSTEM

The only radar in Germany, capable to observe noncooperative objects in space, is the Tracking and Imaging Radar (TIRA) system of FGAN–FHR. It is located about 20 km south of Bonn. A photography of the ring building housing TIRA is shown in Fig. 1.
TIRA consists of three major subsystems:

- *34-m parabolic antenna*, fully computer controlled azimuth-over-elevation pedestal.
- L-band narrowband monopulse *tracking radar* allowing closed-loop target tracking with 1.5 MW, 1 ms pulse length, 30 Hz PRF, gaining for every pulse target range, range rate, azimuth and elevation angles and complex echo amplitude.
- High range-resolution Ku-band *imaging radar*: single-horn imaging radar (guided by tracking radar) with curr. 800 MHz bandwidth (18 cm range resolution) and up to 400 Hz PRF.

Figure 1: Photography of the TIRA system (radome opened).

Some important parameters of the system are given in Table 1. TIRA's coverage for various orbital altitudes is illustrated in Fig. 2
TIRA was initially constructed about 1965 to assist experimental radar research for ABM warning. Since the reentry of KOSMOS–954 in January 1978, FGAN was regularly requested to advice the Federal Minister of Interior in matters of decaying high risk space objects. Today TIRA is mainly used as an experimental system for supporting the development and test of modern radar techniques for space reconnaissance.
Major application areas may be categorized as

- high precision orbit determination (mission support, close encounter predictions, re-entry prediction support,...)

- damage/fragmentation and attitude analysis of satellites
- target cluster analysis
- data assessment for air/space target identification and classification
- observation and analysis of the space debris and meteoroid environment

FGAN may take third-party study contracts with industry, agencies and universities; long cooperation exists e.g. with ESA/ESOC and NASA.

Table 1: Some parameters of the TIRA system.

| Parameter | L–Band Tracking Radar | Ku–Band Imaging Radar |
|---|---|---|
| Centre Freq. | 1333 MHz | 16700 MHz |
| Wavelength | 22.5 cm | 1.8 cm |
| Bandwidth | 250 kHz | 800 MHz |
| Modulation | BPSK | LFM-Chirp |
| Transmit pol. | right circ. | right circ |
| Receive pol. | left circ. | left or right circ. |
| Antenna system | 34-m Parabol, Cassegrain | |
| Angular res. | $0.000172^o$ | |
| Feed system | 4-Horn Monopulse | corrugated horn |
| Antenna gain | $49.7 \pm 0.5$ dB | $73.2 \pm 0.5$ dB |
| 3dB–beamwidth | $0.49^o$ | $0.031^o$ |
| Pulse peak power | 1...2 MW | $< 13$ kW |
| Pulse length (typ.) | 1 ms | 256 $\mu$s |
| Pulse rate | $< 40$ Hz | $< 1.5$ kHz |

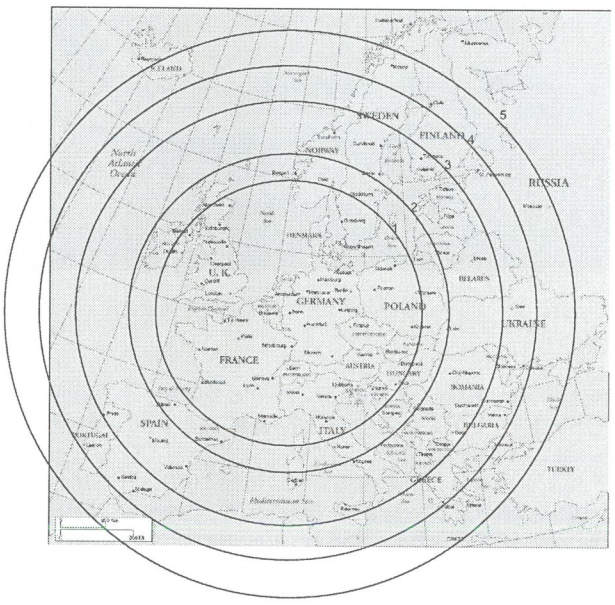


Figure 2: Coverage of the TIRA system for various orbital altitudes: 80 km (1), 120 km (2), 200 km (3), 265 km (4), 340 km (5).

## 2. RADAR IMAGING

Radar imaging is a well established method for non-cooperative reconnaissance of space objects. Due to its 800 MHz bandwidth the Ku-band imaging radar of TIRA currently provides a range independent slant range resolution of 18 cm (25 cm with Hamming windowing). According to the inverse synthetic aperture radar (ISAR) principle, the cross range resolution is provided by Doppler frequency analysis and is mainly determined by the processed synthetic aperture, i.e. the target aspect angle changes during the processing interval. For a square resolution cell of 25 cm x 25 cm the necessary aperture angle is about $2.7^o$.
With respect to the radar station the satellite is in general rotating with a total angular velocity of $\vec{\omega}_{tot} = \vec{\omega}_{trans} + \vec{\omega}_{intr}$, where $\vec{\omega}_{trans}$ is due to the translational motion and $\vec{\omega}_{intr}$ due to the intrinsic rotation of the satellite. This situation is illustrated for a model satellite in pure translational motion (Fig. 3) and with additional intrinsic rotation (Fig. 4).

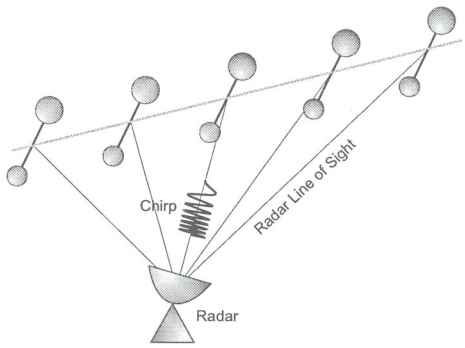


Figure 3: Aspect angle geometry for a (model) satellite in stable flight attitude.

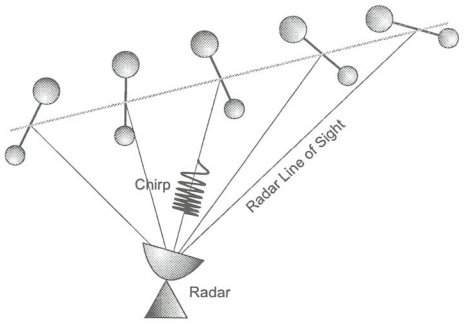


Figure 4: Aspect angle geometry for a (model) satellite with additional intrinsic rotation.

The perpendicular component of the total angular velocity $\vec{\omega}_{tot\perp}$ with respect to the Radar Line of Sight (RLOS) determines the cross range scaling of ISAR images.
A correct estimation of $\vec{\omega}_{tot}$ is necessary, since the component $\vec{\omega}_{tot\perp}$ which is perpendicular to the Radar Line of Sight (RLOS) determines the location and direction of the image plane and the cross range scaling. This is illustrated in Figs. 5-6, where a $|\vec{\omega}_{tot\perp}|$ of $0.25°/s$ and $0.80°/s$ has been assumed, respectively.

elation between $|\vec{\omega}_{tot\perp}|$ and cross range: **ross range scaling** $\sim \frac{1}{|\vec{\omega}_{tot\perp}|}$.
his prevents the direct determination of the intrinsic mo-on of satellites from single ISAR images in general.

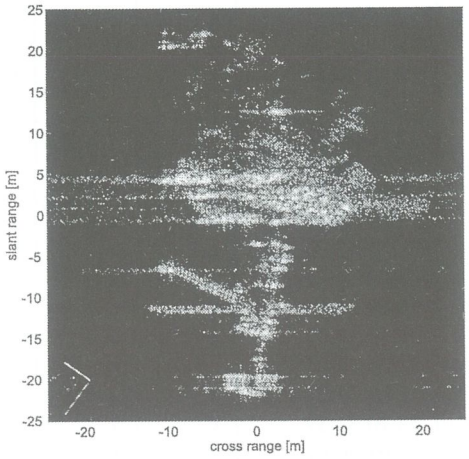


igure 5: Radar image of MIR with an assumed $|\vec{\omega}_{tot\perp}| = .25°/s$.

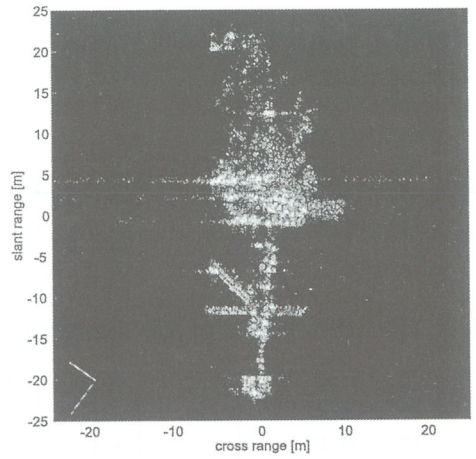


Figure 6: Radar image of MIR with an assumed $|\vec{\omega}_{tot\perp}| = 0.80°/s$.

In case of satellites with known shape and dimensions superposition of suitable wire grid models to a sequence of radar images can help in the estimation of the intrinsic motion parameters. In general however this is a time consuming "try and error" method and gives in most cases no unique solution. An example is given in Figs. 7-9. Fig. 7 shows a wire grid model of MIR derived from the official information published on the TsUP website (Fig. 10). In Fig. 8 a $|\vec{\omega}_{tot\perp}|$ value given by the translational motion only is assumed. Radar image and wire grid do not fit very well. $|\vec{\omega}_{tot\perp}|$ is changed (thus taking intrinsic rotation into account) until image and grid model fit reasonably (Fig. 8). If the intrinsic rotation is simple (e.g. only about a single inertially fixed axis) this "optimum" $|\vec{\omega}_{tot\perp}|$ can then be used for subsequent images.

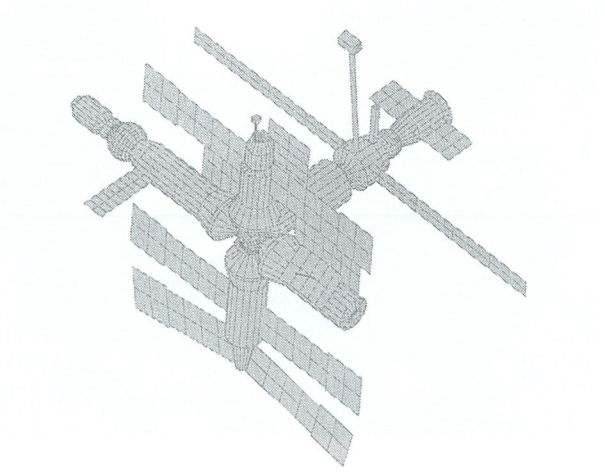

Figure 7: Wire grid model of MIR.

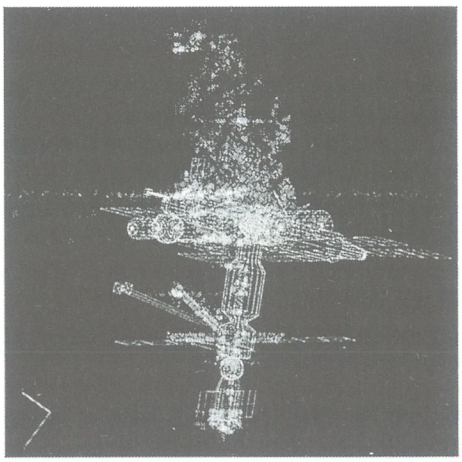

Figure 8: Superposition of wire grid model and radar image with non-optimum $|\vec{\omega}_{tot\perp}|$.

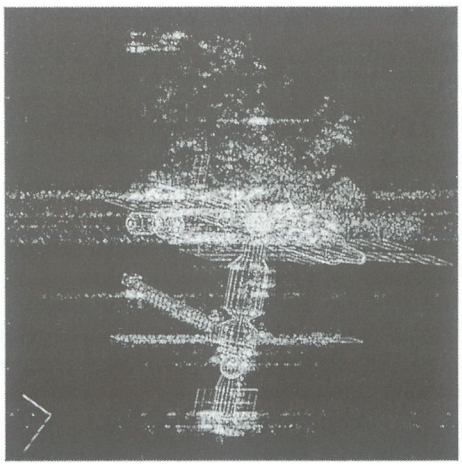

Figure 9: Superposition of wire grid model and radar image with "optimum" $|\vec{\omega}_{tot\perp}|$.

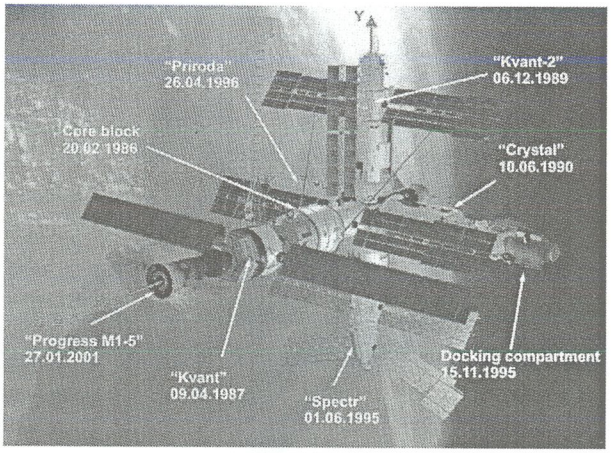


Figure 10: Official MIR configuration (source: TsUP website).

## 3. TIRA OBSERVATIONS OVERVIEW

Three major phases were defined for the participation of TIRA in the MIR deorbiting campaign:
**Phase A** (before Feb 16) *Preparation* phase prior to full implementation of drop-box at ESOC

- testing of tracking, imaging and data preparation procedures
- measurements for assessing current configuration of MIR for later change detection
- implementation of fast, automated routines for data preparation and transfer

**Phase B** (Feb 16 - Mar 9) *Routine tracking* phase

- MIR spin-stabilised (X-axis, $T_x < 30$ min.), moderate decay rate
- routine tracking and imaging, 6...10 passes/week for maintaining TLE database
- quick-look image processing for change notification

**Phase C** (Mar 12 - Mar 23) *Final* phase

- MIR in complex rotation (X-axis + Y-axis, $T_y < 6$ min., decreasing), high decay rate
- dense tracking and imaging schedule, measurements on each day, final 4 days: each visible pass
- image fine-processing for intrinsic motion estimation necessary

Phase C was mainly characterized by the complex rotation of MIR, the analysis of which was not longer possible with the radar image quick-look processor used so far, but forced the application of a more sophisticated and accurate but slow image processor, putting a heavy workload on MIR's attitude analysis.
Tables 2 - 4 list all TIRA observations of MIR during the three campaign phases. Given are date and start time (UTC) of each observed passage. Columns 'TLE', 'RAD' and 'IMA' are marked with an 'x' if a high quality element set (two-line elements), an observation vector sequence (time, azimuth, elevation, range, SNR) and/or

Table 2: TIRA observations of MIR during phase A.

| Date | Time (UTC) | TLE | RAD | IMA |
|---|---|---|---|---|
| 17.1. | 17:10:13:45 | x | x | x |
| 17.1. | 17:11:47:01 | x | x | x |
| 17.1. | 17:13:21:17 | x | x | x |
| 18.1. | 18:10:22:43 | x | x | x |
| 18.1. | 18:13:29:48 | x | x | x |
| 19.1. | 19:08:57:37 | x | x | x |
| 19.1. | 19:10:30:22 | x | x | |
| 19.1. | 19:12:04:18 | x | x | |
| 22.1. | 22:07:48:12 | x | x | |
| 23.1. | 23:09:28:45 | x | x | x |
| 23.1. | 23:11:03:00 | x | x | x |
| 25.1. | 25:08:10:19 | x | x | x |
| 26.1. | 26:09:51:54 | x | x | x |
| 30.1. | 30:10:19:39 | x | x | x |
| 1.2. | 32:08:58:04 | x | x | |
| 1.2. | 32:09:02:23 | x | x | x |
| 1.2. | 32:10:32:39 | x | x | x |
| 2.2. | 33:07:30:02 | x | x | x |
| 2.2. | 33:09:04:01 | x | x | x |
| 2.2. | 33:10:39:12 | x | x | x |
| 5.2. | 36:06:12:30 | x | x | x |
| 5.2. | 36:07:46:35 | x | x | x |
| 5.2. | 36:09:21:07 | x | x | x |
| 7.2. | 38:06:22:51 | x | x | x |
| 7.2. | 38:07:56:11 | x | x | x |
| 9.2. | 40:04:56:35 | x | x | x |
| 9.2. | 40:06:30:32 | x | x | |
| 12.2. | 43:03:33:18 | x | x | |
| 12.2. | 43:05:07:12 | x | x | |
| 14.2. | 45:02:05:16 | x | x | |
| 14.2. | 45:03:39:04 | x | x | |

Table 3: TIRA observations of MIR during phase B.

| Date | Time (UTC) | TLE | RAD | IMA |
|---|---|---|---|---|
| 16.2. | 47:02:09:49 | x d | x d | |
| 16.2. | 47:03:43:28 | x d | x d | |
| 19.2. | 50:00:40:14 | x d | x d | |
| 19.2. | 50:02:13:51 | x d | x d | |
| 22.2. | 52:20:01:02 | x d | x d | x d |
| 22.2. | 52:21:34:13 | x d | x d | x |
| 24.2. | 54:19:59:56 | x d | x d | x |
| 24.2. | 54:21:33:29 | x d | x d | x |
| 26.2. | 57:18:22:18 | x d | x d | x |
| 26.2. | 57:19:55:30 | x d | x d | x |
| 28.2. | 59:18:17:17 | x d | x d | x |
| 28.2. | 59:19:50:43 | x d | x d | x |
| 2.3. | 61:16:37:22 | x d | x d | x |
| 2.3. | 61:18:10:33 | x d | x d | x |
| 5.3. | 64:14:51:03 | x d | x d | x |
| 6.3. | 65:14:45:03 | x d | x d | |
| 7.3. | 66:14:38:39 | x d | x d | x |
| 8.3. | 67:16:04:51 | x d | x d | x |
| 9.3. | 68:14:24:29 | x d | x d | x d |

Table 4: TIRA observations of MIR during phase C.

| Date | Time (UTC) | TLE | RAD | IMA |
|---|---|---|---|---|
| 12.3. | 71:12:25:23 | x d | x d | |
| 15.3. | 74:13:25:01 | x d | x d | x |
| 15.3. | 74:14:58:06 | x d | x d | x |
| 16.3. | 75:10:07:32 | x d | x d | x |
| 16.3. | 75:11:39:39 | x d | x d | x |
| 18.3. | 77:12:44:30 | x d | x d | x |
| 19.3. | 78:09:24:06 | x d | x d | x |
| 19.3. | 78:10:56:25 | x d | x d | x |
| 19.3. | 78:12:29:09 | x d | x d | x |
| 19.3. | 78:14:01:45 | x d | x d | x |
| 20.3. | 79:07:36:50 | x d | x d | |
| 20.3. | 79:09:07:42 | x d | x d | x |
| 20.3. | 79:10:40:00 | x d | x d | x |
| 20.3. | 79:12:12:36 | x d | x d | x |
| 20.3. | 79:13:45:13 | x d | x d | x |
| 21.3. | 80:07:18:56 | x d | x d | |
| 21.3. | 80:08:49:55 | x d | x d | x |
| 21.3. | 80:10:22:18 | x d | x d | x |
| 21.3. | 80:13:27:30 | x d | x d | x |
| 22.3. | 81:06:59:46 | x d | x d | x |
| 22.3. | 81:08:30:48 | x d | x d | x |
| 22.3. | 81:10:03:00 | x d | x d | x |
| 22.3. | 81:11:35:31 | x d | x d | x |
| 22.3. | 81:13:07:57 | x d | x d | x |
| 23.3. | 82:06:08:44 | | | |

a radar image (sequence), respectively could be sucessfully gained. If these data have been transfered to the ESOC drop-box, these columns are additionally marked with a 'd'.
Tab. 5 and Tab. 6 finally provide a summary of all TIRA measurements and data sets transmitted to the drop-box respectively.

Table 5: Summary of TIRA observations of MIR in 2001.

| Observation Phase | Tracking | Imaging |
|---|---|---|
| **A** (Jan 17 - Feb 15) | 31 | 23 |
| **B** (Feb 16 - Mar 09) | 24 | 15 |
| **C** (Mar 12 - Mar 23) | 29 | 21 |
| total | 84 | 59 |

Table 6: Summary of TIRA data and information transfered to ESOC drop-box.

| Type of Data/Information | Dropped |
|---|---|
| **TLE** - Element Sets | 41 |
| **RAD** - Observation vector sequences | 41 |
| **IMA** - Radar images/sequences | 4 |
| **NEWS** - Attitude information | 9 |

## 4. EXAMPLE RESULTS

In the following some results achieved from tracking data and radar image analysis are presented, illustrating selected events during the final 2 month of MIR.
Figure 11 shows a L-band RCS signature (radar cross-section vs. time) from a measurement on Jan 17, 10:13:45, which is typical for MIR in a stable flight attitude. A corresponding radar image from the same pass is shown in Fig. 12. Progress M43 is still docked to the KVANT-1 module of MIR.

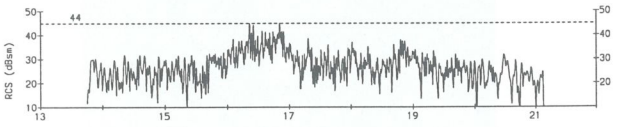


Figure 11: L-band RCS signature on Jan 17, 10:13:45

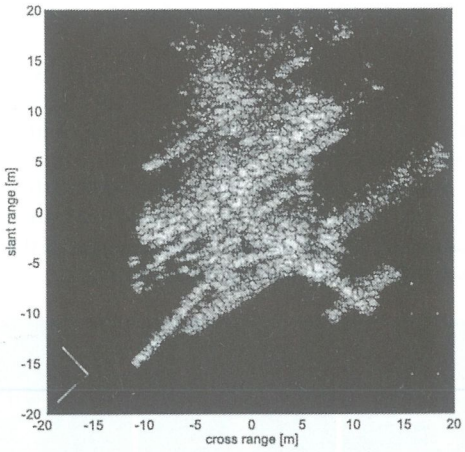


Figure 12: Radar image on Jan 17, 10:14:21

In preparation for the docking of the Progress M1-5 deorbiting spacecraft, Progress M43 was separated from MIR and deorbited. Fig. 13 shows a radar image on Jan 25 with the KVANT-1 front-end free for the docking of Progress M1-5.

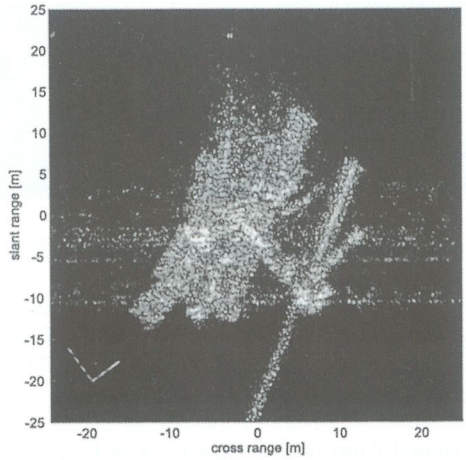


Figure 13: Radar image on Jan 25, 08:10:07

The sucessful docking of Progress M1-5 on Jan 27 is illustrated by Fig. 14.

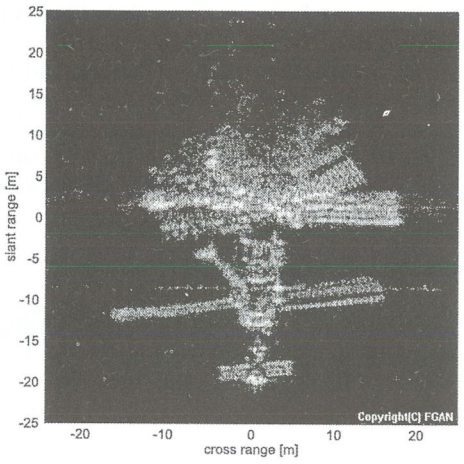


Figure 14: Radar image on Jan 30, 10:19:52

After docking of the Progress module MIR was forced into a slow rotation about the X-axis (SOYUZ docking compartment – KVANT-1, see also Fig. 10) with a period of less than about 30 min. The image sequence in Fig. 15 reveals that even 5 weeks later, on Mar 09, this X-axis spin was the only observable intrinsic motion of MIR. The major part of the aspect angle change in the image sequence is due to the translational motion.

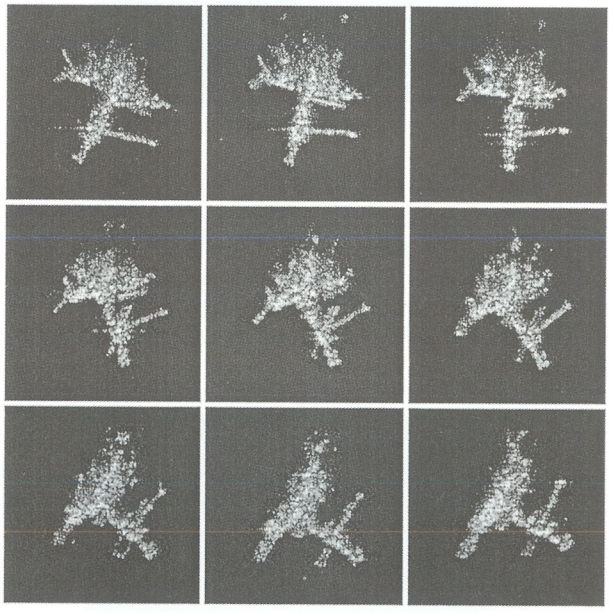

Figure 15: Radar image sequence on Jan 30, 14:25:07.

Between Mar 09 and Mar 15 a sudden additional rotation about an axis nearly parallel to the Y-axis (SPECTR – KVANT-2) occured. Due to problems of the TIRA system during this period, the exact date of this event could not be assessed. On Mar 15 the period of the Y-rotation was estimated from image sequences and radar films as $T_y \approx 4$ min. The rotation rate was steadily increasing until Mar 21, when on the last pass visible to TIRA in the afternoon, $T_y$ already was smaller than about 150 s. Changes were also visible in the RCS signatures (Fig. 16), showing now periodic features from which the estimated rotation period was also confirmed.

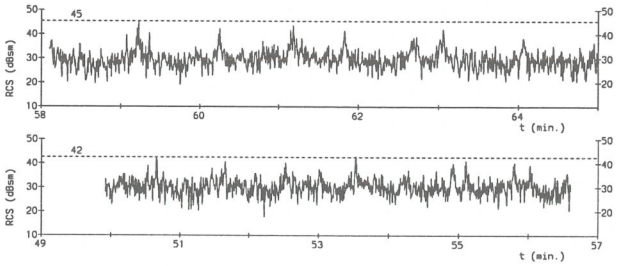


Figure 16: L-band RCS signatures on Mar 15, 14:58:06 (top) and Mar 21, 08:49:55 (bottom).

In the early morning of Mar 22 re-stabilization of MIR was sucessfully performed. The RCS signature taken on the first visible pass (Fig. 17) resembles again the typical shape observed for many years before with MIR in a stable attitude (see also Fig. 11).

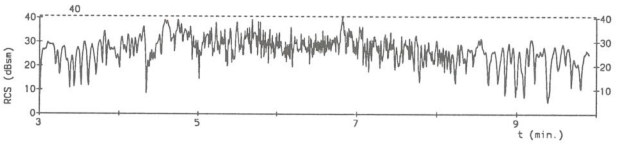


Figure 17: L-band RCS signature on Mar 22, 10:03:00.

During a final 45 min. search on the post-decay orbit starting on Mar 23, 06:08:44 MIR or any parts of it could not be detected again, which lead to the later on confirmed assumption that Mir was sucessfully deorbited as planned.

## 5. CONCLUSIONS

- Assessment of MIR orbital data (TLE, tracking vectors) without problems (sometimes loss of target at very high elevation passes); data available in ESOC drop-box within 2 - 5 min after experiment.
- Imaging data could not be gained on every observed pass due to frequent hardware problems of Ku-band receiver (several low-noise amplifiers burned); quality of Ku-band data not always as expected.
- Image analysis expenditure moderate with quick-look processor, very high when high-quality fine-processor must be used (especially in Phase C - MIR in complex rotation); results available not before 1 hour after experiment.
- Complete intrinsic motion assessment very difficult for MIR, since $\omega_{trans}$ and $\omega_{rot}$ on same order; still unsolved at FGAN.
- Experiences with data exchange procedures (drop-box) were very positive; this instrument should be used for future similar campaigns.